Measurement of pressure fluctuations inside a model thrust bearing using PVDF sensors

Andrew Youssef[1], David Matthews[2,1] Andrew Guzzomi[1], Hongmei Sun[1] and Jie Pan[1]

[1] School of Mechanical and Chemical Engineering, The University of Western Australia, Crawley, Australia
[2]Defence Science and Technology, HMAS Stirling, Rockingham Australia

ABSTRACT

A good understanding of the effect of thrust bearings on the vibrational characteristics of a marine propulsion system is vital in order to develop an accurate model of the drivetrain and to implement vibration control. To achieve this it is necessary to have detailed information about the stiffness and damping of the oil layer inside the bearing and the changes that will occur due to the pressure loading of the oil when the bearing is under load. A simple thrust bearing was thus designed and constructed to emulate features that would be found in a conventional thrust bearing. In doing so, it was possible to incorporate four PVDF sensors into the bearing that could directly measure the pressures generated inside the oil under various conditions. Using this setup, the effects of shaft rotational speed and thickness of the oil film on the pressure were measured. In order to simulate axial vibration effects on the pressure, the thrust bearing was subjected to sinusoidal vibration in the axial direction by directly attaching it to an electro-mechanical shaker.

1. INTRODUCTION

Thrust bearings have a variety of applications but their predominant use is in marine propulsion systems that allow the thrust load produced by the propeller to be transmitted efficiently into the ship's hull, a simple diagram of the system is shown in Figure 1. Knowledge of the condition of the thrust bearing is vital as failure can lead to catastrophic consequences for the whole system. A significant contribution of the overall vibration of the marine propulsion system originates from the propeller operating in a non-uniform wake. These vibrations are transmitted down the shaft, through the thrust bearing and into the hull. The amount of noise transmitted into the hull is highly dependent upon the thrust bearing's stiffness (Youssef et al., 2015, Pan et al., 2002, Dylejko, 2007, Dylejko et al., 2007) and having an accurate model would be highly desirable for both passive and active control of the propeller induced noise. Previous studies (Dylejko, 2007, Dylejko et al., 2007, Gan-bo and Yao, 2012, Stoy, 1948) have modelled the stiffness using a linear model for the thrust bearing, however there is evidence to suggest that the thrust bearing experiences nonlinear behaviour under certain conditions (Pan et al., 2002, Murawski, 2004). It would therefore be desirable to have a sensor that could directly monitor the contact force inside the thrust bearing itself. Such a device would ideally need to be very thin such that it does not require significant modification of the thrust bearing in order to be embedded. Using conventional accelerometers would be very difficult. One suitable alternative however is Polyvinylidene Fluoride (PVDF) a piezoelectric polymer film. This paper will report on results that directly measure the pressure developed by the thrust bearing and determine the stiffness using PVDF sensors.

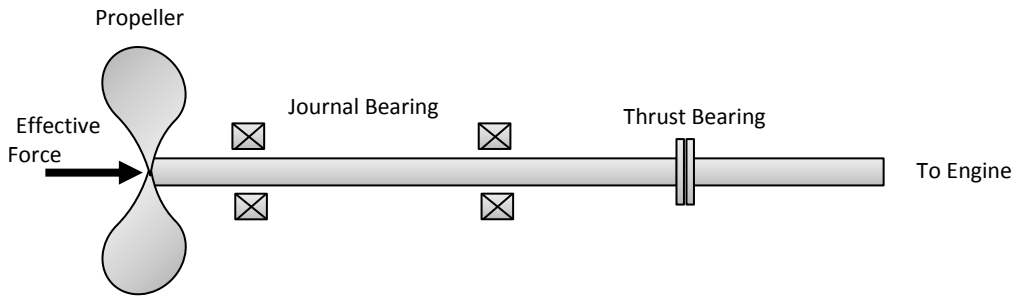

Figure 1: Diagram of system.

2. DESCRIPTION OF EXPERIMENTAL SETUP

PVDF is a chemically inert polymer which becomes piezo-electric when polarized in an electric field. It was discovered in 1969 by Kawai (Kawai, 1969) and, since then has been used for a number of pressure sensing capabilities (Shirinov and Schomburg, 2008, Lee and Sung, 1999, Mahale et al., 2011). Its thin flexible characteristics together with its ease of use and inert properties make it an ideal candidate for use as a pressure sensor inside an oil-filled environment such as a thrust bearing.

The PVDF used in this work are SDT1-D28 films and have an active area of 13 mm by 30 mm with a film thickness of 28 μm. The films come doubled over to reduce EM noise giving an overall thickness of 56 μm. They have been polarised in their thickness direction referred to as the d_{33} mode. The films are supplied with attached shielded cables and were terminated with a SMB connector to minimise unwanted noise.

A model thrust bearing housing was designed and constructed using a 3D printer. A diagram is shown in Figure 2(a). The bearing housing has an inner diameter of 120 mm and a height of 40 mm and was made out of Stratasys 720 Full Cure ink. Recesses were made in the base to accommodate four PVDF films. The coaxial cables from each film were fed through the sides of the housing as shown in the diagram. The films were secured to the base using superglue and then covered with epoxy up to the level of the base. This resulted in a flat base surface with four embedded PVDF films. The housing was attached to a large mechanical shaker that was used to investigate the effects of various vibrations on the output of the PVDF

The upper half of the thrust bearing model consisted of a smooth steel piston of diameter 100 mm and height 200 mm, which could be inserted into the housing and held at various heights above the PVDF film. The piston could be rotated about its axis at various speeds up to 300 rpm using an electric motor mounted directly above. A photo of the complete setup is shown in Figure 2(b).

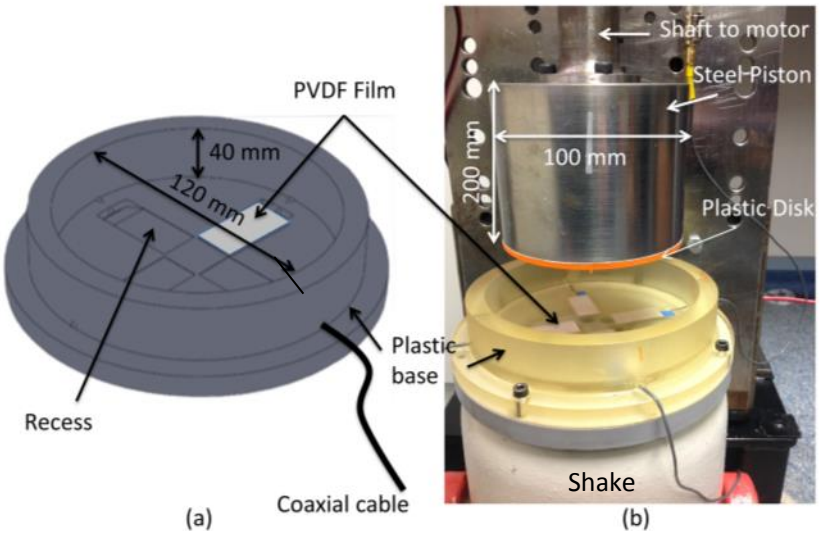

Figure 2: Schematic of model thrust bearing (a) and photograph of entire experimental setup (b)

Three thin plastic disks with different pad designs were fabricated using a 3D printer (orange disk in Figure 2b) and were attached to the base of the piston using double sided sticky tape. This may introduce unwanted compliance and damping properties into the system. However, this is a proof of concept and this will be addressed in future work. Using this fabrication method it was possible to easily change the shape and size of the pads to get a better understanding of the developed pressure field inside the bearing. Three bearing designs were investigated. The first was a generic four pad bearing with a tilt of 5°. Each pad covered an angle of 45° with a gap of 45° between each. The height at the outer and inner radius was 3.6 mm and 0.5 mm respectively and the length of each pad was 30 mm. The second and third discs had protrusions that were rectangular in cross section. Both were 3.0 mm high and 30 mm long. The width of the step for disc 2 and 3 was 1 mm and 13 mm respectively. Schematic of the designs are shown in Figure 3.

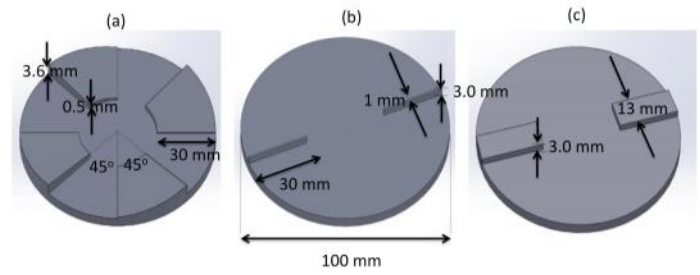

Figure 3: (a) Angled pad, (b) 1mm wall and (c) 13 mm wall

The piston/pad assembly was suspended inside the bearing housing which was filled with Castrol 445 motor oil. Although typical thrust bearings tend to use thicker grade of oils, this grade of oil was chosen as the system being tested was subjected to small loads. The distance between the pads and the PVDF films was carefully controlled and the piston rotated at various speeds from 0 to 300 rpm. The rotational speed and position of the pads relative to the PVDF films was monitored using tachometer and a piece of reflective tape attached to the side of the piston.

The output from each sensor was amplified with 20 dB of gain using a B&K 2635 charge amplifier. The signals were then digitised using a LAN-XI Type 3050 data acquisition module and post-processed using MatLab.

3. RESULTS AND DISCUSSION

The output of the PVDF sensors are given in volts which is directly proportional to the strain applied to the sensors. As the sensors are embedded in the thrust bearing housing, the strain corresponds to the change in thickness direction (i.e. the d_{33} mode) of the PVDF sensors which is proportional to the distributed pressure on them. The variability in sensor sensitivity was checked by comparing the peak voltage observed from the sensors when struck with an impact hammer to the output of the hammer.

Initial measurements were done using the simple step bearing pads with rectangular cross sections discussed above. Figure 4 shows the result of the 1 mm and 13 mm stepped pad bearing where (b) shows the signal output from one of the PVDF films for both pads rotating at 300 rpm. The blue curve shows the results for the 1mm pad and the green for the 13 mm pad. The height between the pads and the PVDF film was 0.5 mm. As can be seen both pads show similar features with the 13 mm pad producing a larger response. The voltage oscillation indicates that the PVDF film is measuring positive and negative pressures (relative to atmospheric pressures) depending on the position of the pads. Figure 4(a) shows the plan view of the bearing housing. The voltage output of only the upper film has been considered. The numbers 1 to 13 around the circumference of the circle show the position of the leading edge of the two pads relative to the upper PVDF film. The corresponding time dependent voltage output of the film is shown in Figure 4(b). For example, position 1 is where the leading edge of the pads crosses the leading edge of the PVDF film. The following conclusions can be made;

(1) The maximum pressure occurs when the leading edge of the pad first starts passing over the PVDF film (position 1). This will be due to a high pressure region that is developed in front of the pad as it pushes the oil.
(2) During the interaction of the pad with the film the voltage steadily decreases. Zero voltage is observed when the pads are directly over the top of the film (where the leading edge of the pad is at point 2). This position is independent of the pad width. For the 13 mm pad in this position the entire area of the film is covered by the pad, for the 1 mm pad, 1/13 of the film's area is covered.
(3) Negative voltages indicate negative pressures experienced by the PVDF.
(4) The maximum negative pressure occurs when the back edge of the pad leaves the PVDF film. This again is independent of the width of the pad.
(5) For the 1mm pad, the maximum and minimum voltages are approximately the same. For the 13 mm pad, the negative voltage is approximately 1.8 times that of the positive value's amplitude.

Physically, the maximum force corresponds to the maximum coverage of the leading edge positive pressure region on the PVDF film, while the maximum negative force corresponds to the maximum coverage of the tailing edge negative pressure region on the PVDF film.

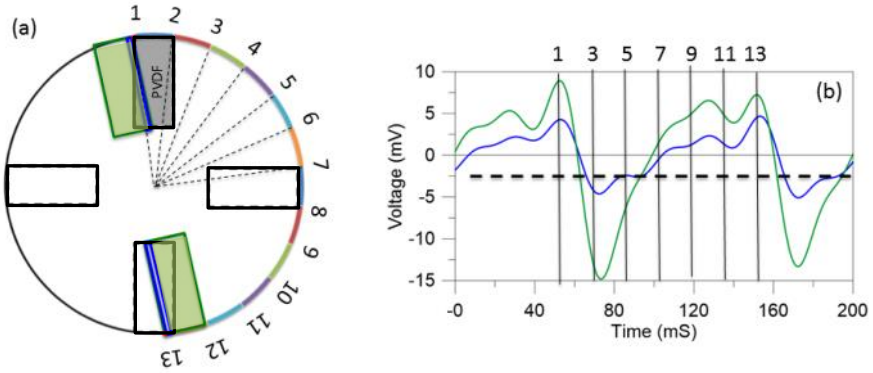

Figure 4: (a) Shows the relative position of the pads (green rectangles) to the PVDF sensors (dashed rectangles). (b) is the time dependent voltage in relation to the position of the leading edge of the pad, where the blue curve is the 1 mm width stepped pad and the green curve is the 13 mm width stepped pad.

Similar measurements were performed for the angled pad at the same speed and height. The results are shown in Figure 5. One main difference between this disk and the previous two is that there are four pads distributed around the disk instead of two. As a result, an extra two peaks are observed in the voltage output for the same time.

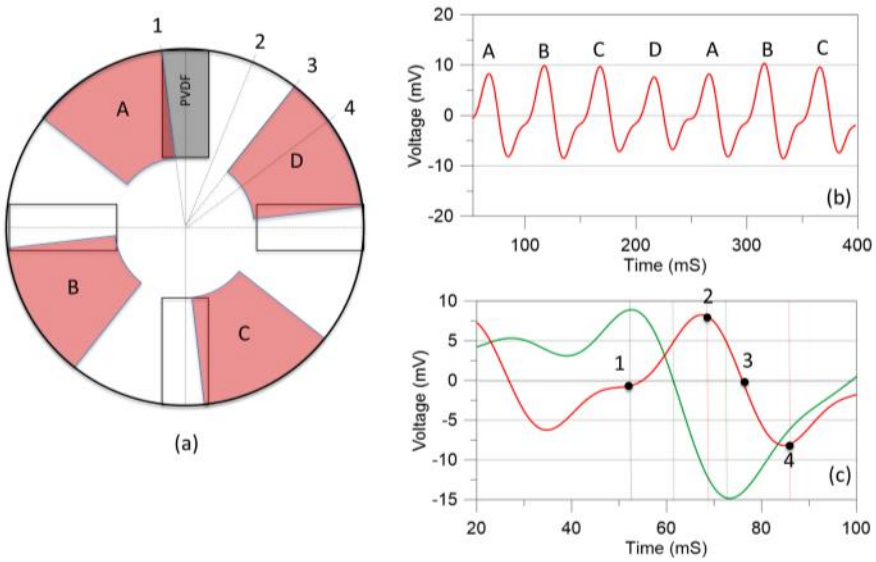

Figure 5: (a) Shows the relative position of the pads (in red) to the PVDF sensors (dashed rectangles). The time dependent voltage output is shown in (b) and comparison between the step pads is shown in (c)

The time dependent voltage output from the top PVDF film is shown in Figure 5(b). The four individual pads have been labelled A, B, C and D and a small variation in the output voltage for each pad can be observed due to misalignments. Figure 5c shows the voltage output from the film for a single pass of a pad. The red curve corresponds to the output for the angled pad and the green curve for the 13 mm step pad. The output from the PVDF sensors at 1, 2, 3, 4 shown in Figure 5a have the corresponding values shown in figure 5c. Comparing Figures 4b and 5b it is clear that a simpler waveform is obtained for the tilted pad then the previous step pads. The following features can be observed;

(1) As the leading edge of the pad passes over the PVDF film zero voltage is observed. Position 1. The voltage then gradually increases as the pad covers the film.
(2) The maximum voltage (which corresponds to maximum pressure) occurs when the pad is directly on top of the PVDF film. Position 2. After this point the voltage starts to drop.
(3) Zero voltage is observed when the trailing edge of the pad first starts leaving the film. Position 3.
(4) Once the back edge of the pad has left the PVDF film a region of negative pressure is observed similar to that observed in the step pad (green). A minimum in pressure is observed at position 4 when the trailing edge first starts to leave the film
(5) The magnitudes of the maximum and minimum voltages are the same.

Stachowiak & Batchelor (Stachowiak and Batchelor, 2013) showed that the pressure profile underneath a tilted pad or a stepped pad is directly proportional to that of the sliding speed of the bearing. All three pad types where spun from 0 rpm, to the maximum allowable speed of the motor of 300 rpm in increments of 50 rpm. The results in Figure 6 confirm that the maximum peak pressure obtained from the PVDF sensors approximately linear and essentially directly proportional to the sliding speed.

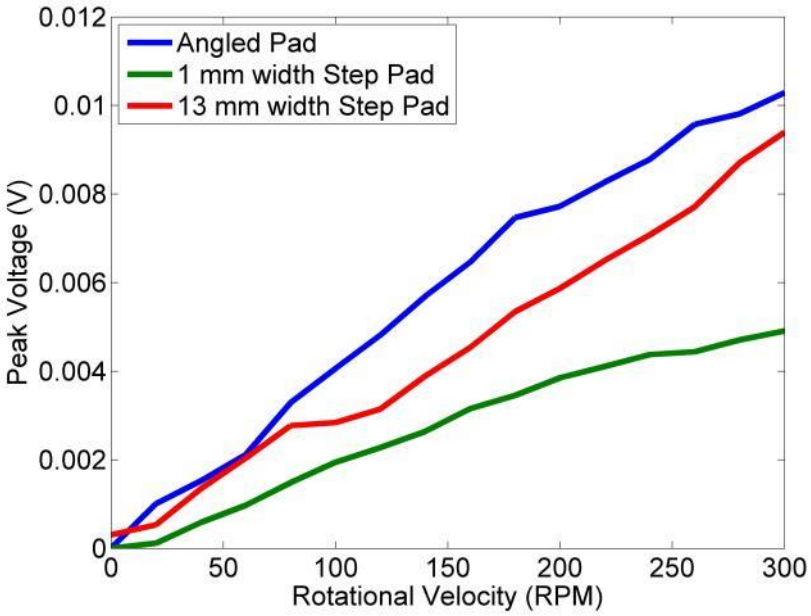

Figure 6 Variation of the peak voltage as a function of rotational speed for all three pads.

In a real thrust bearing under normal operating conditions the bearing is subjected to propeller induced vibrations transmitted via the propeller shaft. In order to try and simulate this the thrust bearing housing was attached to an electromagnetic shaker that could be driven at various frequencies and amplitudes (see Figure 2b). In doing so it was possible to investigate the effect of the vibration on the stiffness of the bearings under various conditions. The results here will focus on the 13 mm step bearing. The rotational speed and height of the pad was fixed at 300 rpm (5Hz) and 0.5 mm respectively. The amplitude of the shaker was set to oscillate between +/- 0.05 mm at each of the frequencies f= 6, 10 and 25 Hz. The acceleration of the bearing housing was carefully monitored using an accelerometer attached directly to it. The voltage output of the PVDF film was then measured at each frequency. The phase between the input and output was not measured.

Given the rotational speed of 5Hz and 2 pads passing a single PVDF sensor per rotation the pad pass frequency is 10Hz. The time dependent output for a 10 Hz excitation frequency is shown in Figure 7b. For comparison the output for the film with zero excitation is shown in Figure 7a. The position of the front of the pad relative to the film has been

shown on the figures similar to that shown in Figure 3. As can be seen the additional vibration results in a more complicated waveform which is the superposition of the vertical vibration of the shaker and the rotating step pad.

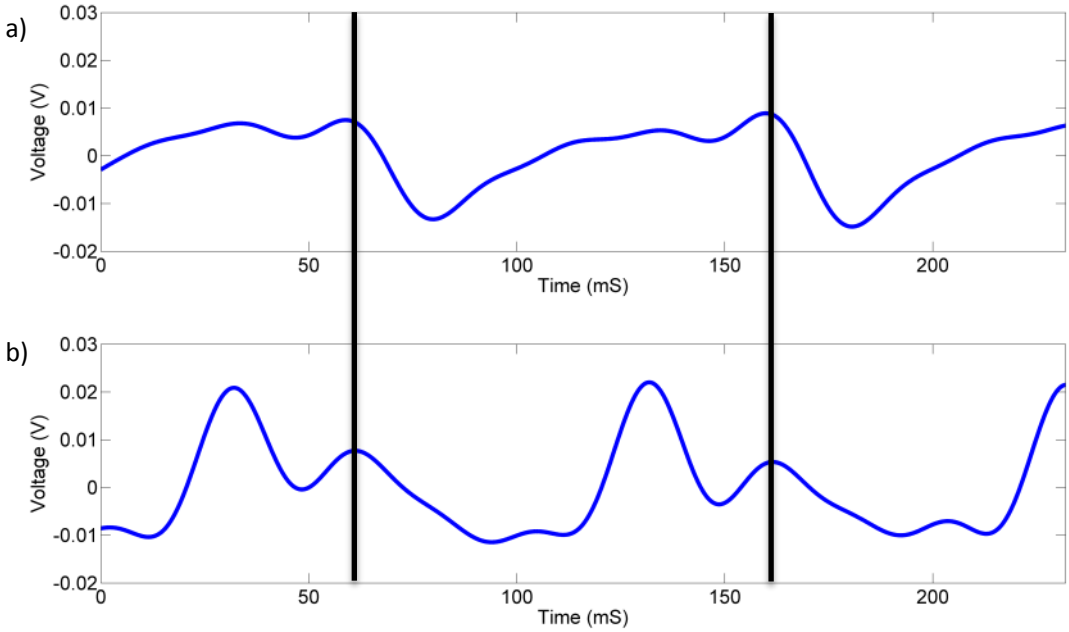

Figure 7: The time dependent output from the PVDF with zero excitation (a) and 10 Hz excitation (b). The position of the leading edge of the pad as it crosses the film is shown by the black lines.

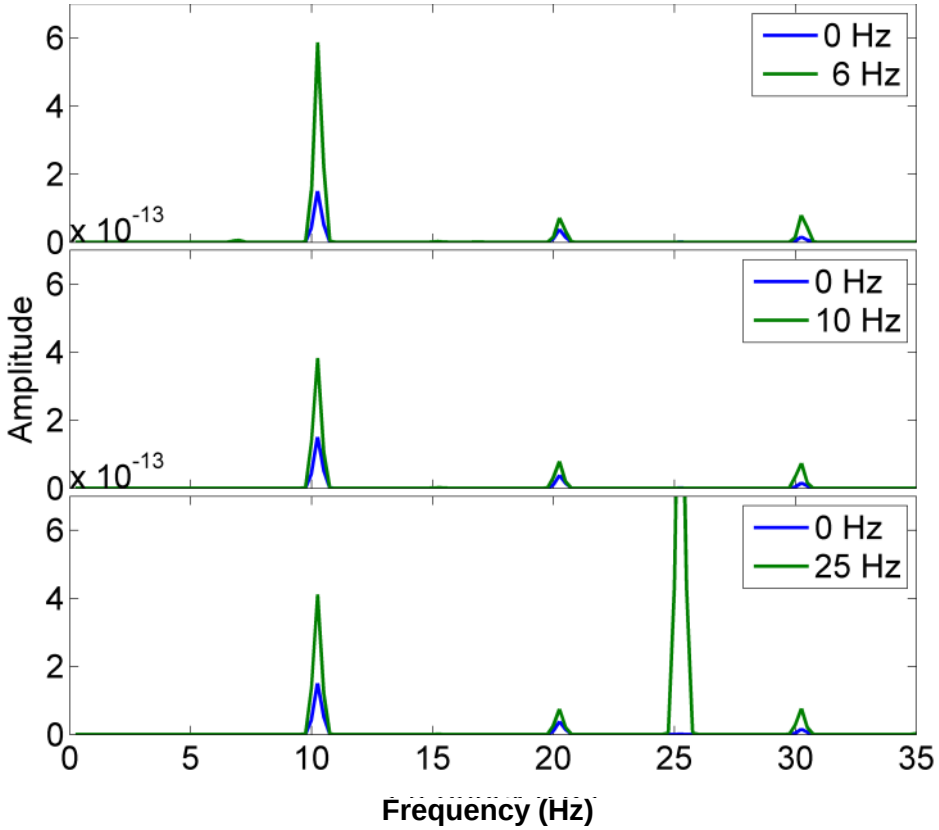

Figure 8: The frequency domain data for no excitation (Blue) and 6 Hz (top), 10 Hz (middle) and 25 Hz (bottom) excitation frequency. All rotational speeds were 6Hz.

To investigate the effect of the vibration on the pressure under the pads an FFT was taken of the time domain data and the amplitude of the 10 Hz frequency monitored for the three excitation frequencies. This is shown in Figure 8. The following features can be observed from Figures 7and 8:

(1) The external excitation significantly influences the frequency content of the voltage response compared to the no excitation output
(2) Peaks are seen at each of the excitation frequencies of 6 Hz (albeit very small), 10 Hz and 25 Hz.
(3) The maximum positive pressure observed by the PVDF sensors has increased due to the excitation at each frequency. This increase is a function of frequency and will depend on the difference between the phase of the excitation and that of the rotation. This will be investigated in future work
(4) The effect of the shaker has negligible effect on the negative pressure as shown by the time domain data.

These observations suggest that the pressure loading generated by the thrust bearing does in fact change with vibration of the system in the axial direction. The vibration of the thrust bearing causes the pressure generated to increase which suggests that both the relative fluctuation between the shaft and bearing housing and the uneven profile contribute to the contact pressure. The effect of these combined excitations on the contact pressure is dependent on the amplitude and frequency of the axial vibration. The relative phase between cyclic rotation of the pads and the axial vibration also is expected to play some role in the resultant pressure. Such effects have been observed in other non-linear dynamic systems experiencing forced vibration(Guzzomi et al., 2010). Future work will therefore focus on the effect of phasing.

It is believed that the change in pressure seen is caused by the change in apparent viscosity of the oil. The oil has a viscosity at a steady state that defines its ability to flow, in a state of continuous vibration these properties would change. To see an increase in pressure developed underneath the pad, the apparent viscosity would have to increase. Further investigation is required to confirm this hypothesis.

4. CONCLUSIONS

A model thrust bearing was constructed using a 3D printer and the pressure variation inside the bearing was successfully measured using thin PVDF film embedded inside the bearing. Various bearing shapes were investigated to fully understand the dynamics of the bearing.

Using the PVDF sensors, it was shown that the stepped pad bearings experiences maximum pressures at the leading edge of the pads, and maximum negative pressure trailing the pads. It was also shown that the pressure signature for a tilted pad is different to that of stepped pads, where the maximum observed pressure was directly underneath the pad. The PVDF sensors where able to show the relationship between the sliding speed of the bearing and the maximum positive pressure being directly proportional. The effect of vibration on the thrust bearing was also investigated, the PVDF sensors where able to showed that there was an increase in the pressure generated by the thrust bearing suggesting an increase in stiffness.

ACKNOWLEDGEMENTS

The first author would like to thank Paul Dylejko for his continued support and Defence Science and Technology for a postgraduate top-up scholarship. Andrew Munyard's help in the 3D printing required for building the model bearing is also acknowledged.

REFERENCES

DYLEJKO, P. G. 2007. *Optimum resonance changer for submerged vessel signature reduction.* PhD Thesis, The University of New South Wales, Sydney, Australia.

DYLEJKO, P. G., KESSISSOGLOU, N. J., TSO, Y. & NORWOOD, C. J. 2007. Optimisation of a resonance changer to minimise the vibration transmission in marine vessels. *Journal of Sound and Vibration,* 300**,** 101-116.

GAN-BO, Z. & YAO, Z. 2012. Reduced-order Modeling Method for Longitudinal Vibration Control of Propulsion Shafting. *IERI Procedia,* 1**,** 73-80.

GUZZOMI, A. L., HESTERMAN, D. C. & STONE, B. J. 2010. Some effects of piston friction and crank or gudgeon pin offset on crankshaft torsional vibration. *Journal of Ship Research,* 54**,** 41-52.

KAWAI, H. 1969. The piezoelectricity of poly (vinylidene fluoride). *Japanese Journal of Applied Physics,* 8**,** 975.

LEE, I. & SUNG, H. I. 1999. Development of an array of pressure sensors with PVDF film. *Experiments in Fluids,* 26**,** 27-35.

MAHALE, B. P., BODAS, D. & GANGAL, S. A. Development of PVDF based pressure sensor for low pressure application. Nano/Micro Engineered and Molecular Systems (NEMS), 2011 IEEE International Conference on, 2011. IEEE, 658-661.

MURAWSKI, L. 2004. Axial vibrations of a propulsion system taking into account the couplings and boundary conditions. *Journal of Marine Science and Technology,* 9**,** 171-181.

PAN, J., FARAG, N., LIN, T. & JUNIPER, R. 2002. Propeller induced structural vibration through the thrust bearing. *Proceedings of the Annual Conference of the Australian Acoustical Society.* Adelaide, Australia; .

SHIRINOV, A. V. & SCHOMBURG, W. K. 2008. Pressure sensor from a PVDF film. *Sensors and Actuators a-Physical,* 142**,** 48-55.

STACHOWIAK, G. & BATCHELOR, A. W. 2013. *Engineering tribology*, Butterworth-Heinemann.

STOY, V. 1948. Longitudinal vibration of marine propeller shafting. *Journal of the American Society for Naval Engineers,* 60**,** 341-365.

YOUSSEF, A., GUZZOMI, A., PAN, J. & DYLEJKO, P. 2015. Preliminary Modelling of A Marine Propulsion System. *Australian Acoustical Society Acoustics 2015 Hunter Valley*.